

Selection and Validation of Mathematical Models of Power Converters using Rapid Modeling and Control Prototyping Methods

Fredy E. Hoyos¹, John E. Candelo², and John A. Taborda³

¹Scientific and Industrial Instrumentation Research Group School of Physics, Universidad Nacional de Colombia, Sede Medellín, Email: fehoyosve@unal.edu.co

²Department of Electrical Energy and Automation, Facultad de Minas, Universidad Nacional de Colombia, Sede Medellín. Email: jecandelob@unal.edu.co

³Faculty of Engineering, Electronics Engineering, Universidad del Magdalena, Santa Marta, Magdalena, Colombia. Email: jtaborda@unimagdalena.edu.co

Article Info

Article history:

Received: Oct 7, 2017

Revised: Mar 9, 2018

Accepted: Apr 1, 2018

Keyword:

DC-DC buck converter
rapid control prototyping
digital PWM

Lyapunov exponents
stability analysis
bifurcation diagrams

ABSTRACT

This paper presents a methodology based on two interrelated rapid prototyping processes in order to find the best correspondence between theoretical, simulated, and experimental results of a power converter controlled by a digital PWM. The method supplements rapid control prototyping (RCP) with effective math tools to quickly select and validate models of a controlled system. We show stability analysis of the classical and two modified buck converter models controlled by zero average dynamics (ZAD) and fixed-point induction control (FPIC). The methodology consists of obtaining the mathematical representation of power converters with the controllers and the Lyapunov Exponents (LEs). Besides, the theoretical results are compared with the simulated and experimental results by means of one- and two-parameter bifurcation diagrams. The responses of the three models are compared by changing the parameter (K_s) of the ZAD and the parameter (N) of the FPIC. The results show that the stability zones, periodic orbits, periodic bands, and chaos are obtained for the three models, finding more similarities between theoretical, simulated, and experimental tests with the third model of the buck converter with ZAD and FPIC as it considers more parameters related to the losses in different elements of the system. Additionally, the intervals of the chaos are obtained by using the LEs and validated by numerical and experimental tests.

Copyright © 2018 Institute of Advanced Engineering and Science.
All rights reserved.

Corresponding Author:

Fredy Edimer Hoyos

Universidad Nacional de Colombia, Sede Medellín

Calle 59A No. 63-20, Medellín, Colombia.

Telephone: (574) 4309327

Email: fehoyosve@unal.edu.co

1. INTRODUCTION

A good mathematical model derives from an appropriate balance between simplicity and accuracy. An approach that combines theoretical, simulated, and experimental tests is pertinent to find the best balance. Advances in electronics have allowed the development of rapid control prototyping (RCP) platforms [1], where real-world systems can be automatically connected with mathematical models [2]. The integration of theoretical, simulated, and experimental methods can be achieved in order to find the best model and validate the control strategy at the same time. In this paper, we illustrate this possibility by means of the analysis of a buck converter.

Digital pulse–wide modulation (DPWM) is now widely used to control power converters because of many advantages such as non-linear control implementation, advanced control algorithms, low power consumption, reduction of external passive components, lower sensitivity to parameter variations, applications for high frequency digital controllers, and others as described in [3, 4, 5, 6].

However, the quantization effects in the state variables and in the duty cycle can cause undesirable limit-cycle oscillations or chaos [7, 8, 9, 10] and delays in the controller produce instability [11]. For these reasons, the dynamic response of digitally controlled DC-DC converters was studied in [3] by the non-uniform quantization. In [7], steady-state limit cycles in DPWM-controlled converters were evaluated and to avoid oscillations some conditions are imposed on the control law and the quantization resolution. The FPIC control technique allows the stabilization of unstable orbits as presented in [12]. Furthermore, the parameter estimation techniques allowed estimating unknown varying parameters of converters [13, 14]. In [4], the minimum requirements for digital controller parameters, namely, sampling time and quantization resolution dimensions are determined. All these techniques demonstrate how to control some unstable events with controllers and have shown some advantages of using the adjustment parameters, but a low number of them have estimated the parameters for the ZAD controllers [5]. Therefore, more research is needed to validate the effects with different parameters and techniques to visualize the stability behaviors.

A better visualization approach has been applied in [15], where the output voltage of a buck power converter is controlled by means of a quasi-sliding scheme. They introduce the load estimator by means of Least Mean Squares (LMS) to make ZAD and FPIC control feasible in load variation conditions and to compare the results for controlled buck converter with SMC, PID and ZAD–FPIC control techniques. However, this work lacks of a complete representation of the stability events and analysis, and a comparison of the different effects that create the control parameters with LEs and bifurcation diagrams. Furthermore, a comparison between numerical and experimental tests is needed to identify the similarities in stability zones, the periodic orbits, the periodic bands, and the chaos.

Therefore, this work presents a stability analysis of three models of buck converters controlled by ZAD and FPIC, with the aim of selecting the best model that represents similar behaviors between the theoretical, simulated, and experimental tests. For this purpose, Section 2 presents the mathematical models of buck converter, Section 3 shows the mathematical model of the ZAD control strategy, and Section 4 illustrates the mathematical model of the FPIC technique. Sections 5, 6, and 7 present the mathematical model for the first, second, and third model of the buck converters, respectively. Section 8 presents the results and analysis, where the comparison of the three models with the theoretical, simulation, and experimental tests are performed. Finally, Section 9 shows the conclusions.

2. MATHEMATICAL MODEL

A complete schematic diagram of the system under study is shown in Figure 1. The converter is formed by a power source E , an internal source resistor r_s , a MOSFET (metal oxide semiconductor field-effect transistor) as a switch S with internal resistance r_M , a diode D with direct polarization voltage V_{fd} , a filter LC , an internal resistance of the inductor r_L , a resistance used to measure the current r_{Med} , and a resistance representing the load of the circuit R [16]. The variables measured in the converter are the capacitor voltage v_c and the inductor current i_L . These variables are measured in real time and they are sent to the ZAD and FPIC in order to calculate a signal for the centered pulse width modulation (CPWM), which closes the control loop.

This system changes the structure with the action of the switch S , which is managed by the CPWM. This modulator consists of a circuit composed of a switch and a DC power source, which in conjunction with the filter LC and the diode D , must supply an average voltage v_c to the output during a switching period. For this effect, the CPWM changes the switch S between the states ON (E) and OFF ($-V_{fd}$). Figure 2 shows the general idea of the CPWM, where d is the duty cycle calculated for each period.

When the control input is $u = 1$, then the state of the switch S is active (ON) and the system gets into a continuous conduction mode (CCM), which can be modeled as in (1).

$$\begin{bmatrix} \dot{v}_c \\ \dot{i}_L \end{bmatrix} = \begin{bmatrix} \frac{-1}{RC} & \frac{1}{C} \\ \frac{-1}{L} & \frac{-(r_s+r_M+r_{Med}+r_L)}{L} \end{bmatrix} \begin{bmatrix} v_c \\ i_L \end{bmatrix} + \begin{bmatrix} 0 \\ \frac{E}{L} \end{bmatrix} \quad (1)$$

This last equation can be simplified and written as in (2).

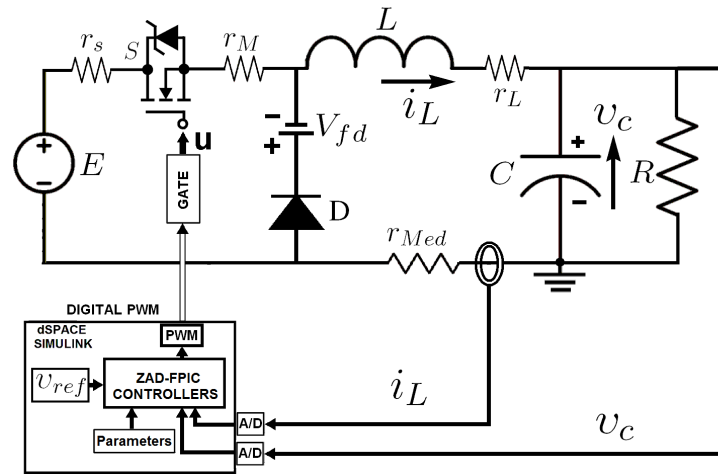


Figure 1. Schematic diagram of the buck converter controlled by the ZAD and FPIC

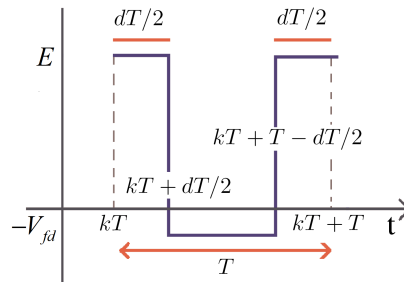


Figure 2. Scheme of a CPWM

$$\begin{bmatrix} \dot{x}_1 \\ \dot{x}_2 \end{bmatrix} = \begin{bmatrix} a & h \\ m & p_2 \end{bmatrix} \begin{bmatrix} x_1 \\ x_2 \end{bmatrix} + \begin{bmatrix} 0 \\ \frac{E}{L} \end{bmatrix} \tag{2}$$

When the control input is $u = 0$, switch S is inactive (OFF) and the system can be modeled as shown in (3).

$$\begin{bmatrix} \dot{v}_c \\ \dot{i}_L \end{bmatrix} = \begin{bmatrix} \frac{-1}{RC} & \frac{1}{C} \\ \frac{-1}{L} & -(r_{Med} + r_L)/L \end{bmatrix} \begin{bmatrix} v_c \\ i_L \end{bmatrix} + \begin{bmatrix} 0 \\ \frac{-V_{fd}}{L} \end{bmatrix} \tag{3}$$

This equation can be simplified and written as in (4).

$$\begin{bmatrix} \dot{x}_1 \\ \dot{x}_2 \end{bmatrix} = \begin{bmatrix} a & h \\ m & p_3 \end{bmatrix} \begin{bmatrix} x_1 \\ x_2 \end{bmatrix} + \begin{bmatrix} 0 \\ \frac{-V_{fd}}{L} \end{bmatrix} \tag{4}$$

where $a = -1/RC$, $h = 1/C$, $m = -1/L$, $p_2 = -(r_s + r_M + r_{Med} + r_L)/L$, $p_3 = -(r_{Med} + r_L)/L$, and $x_1 = v_c$, $x_2 = i_L$. The notation $x_1 = v_c$ represents the capacitor voltage or the voltage at the load bus, and $x_2 = i_L$ represents the current through the inductor.

The state equations (2) and (4) have been simplified as shown in (5); where $\dot{x} = [\dot{x}_1, \dot{x}_2]'$ = $[\frac{dx_1}{dt}, \frac{dx_2}{dt}]'$. In the input matrices B_1 and B_2 is the information of the control inputs according to the scheme of the CPWM (Figure 2).

$$\dot{x} = \begin{cases} A_1x + B_1 & \text{if } kT \leq t \leq kT + dT/2 \\ A_2x + B_2 & \text{if } kT + dT/2 < t < kT + T - dT/2 \\ A_1x + B_1 & \text{if } kT + T - dT/2 < t < kT + T \end{cases} \tag{5}$$

The next step is to design a control strategy that allows the capacitor voltage ($x_1 = v_c$) to be equal to the reference voltage x_{1ref} or a desire value. To obtain tracking or regulation, the time must be calculated

with a predefined period T , in which the switch S must remain closed ($u = 1$), called the “duty cycle” d , with ($d \in [0, T]$). Thus, the duty cycle d is defined as the time that the switch S is closed for the period T .

3. ZAD CONTROL STRATEGY

This control technique was proposed by [17], and tested numerically and experimentally in [15, 18, 19]. This technique basically consists of defining a function and force an average value of zero at each sampling period. For this particular case, $s(t)$ is used as a function of the state value at the start of the sampling period $s(x(kT))$. In this case, the function is defined as a linear function (Figure 3) and slopes are obtained from the values of the state variables in the instant of sampling $t = kT$ as shown in (6) and (7). The function $s(x(kT))$ is linear in its sections, as shown in Figure 3 and it can be expressed as in (6).

$$s(\mathbf{x}(kT)) = \begin{cases} s_1 + (t - kT)\dot{s}_+ & \text{if } kT \leq t \leq kT + \frac{dT}{2} \\ s_2 + (t - kT - \frac{dT}{2})\dot{s}_- & \text{if } kT + \frac{dT}{2} < t < kT + (T - \frac{dT}{2}) \\ s_3 + (t - kT - T + \frac{dT}{2})\dot{s}_+ & \text{if } kT + (T - \frac{dT}{2}) \leq t \leq (k+1)T \end{cases} \quad (6)$$

where

$$\begin{aligned} \dot{s}_+ &= (\dot{x}_1 + k_s \ddot{x}_1) \Big|_{x=x(kT), S=\text{ON}} \\ \dot{s}_- &= (\dot{x}_1 + k_s \ddot{x}_1) \Big|_{x=x(kT), S=\text{OFF}} \\ s_1 &= (x_1 - x_{1ref} + k_s \dot{x}_1) \Big|_{x=x(kT), S=\text{ON}} \\ s_2 &= \frac{d}{2} \dot{s}_+ + s_1 \\ s_3 &= s_1 + (T - d)\dot{s}_- \end{aligned} \quad (7)$$

where $k_s = K_s \sqrt{LC}$ and the term K_s is a constant of the controller and considered as a parameter in the bifurcation analysis.

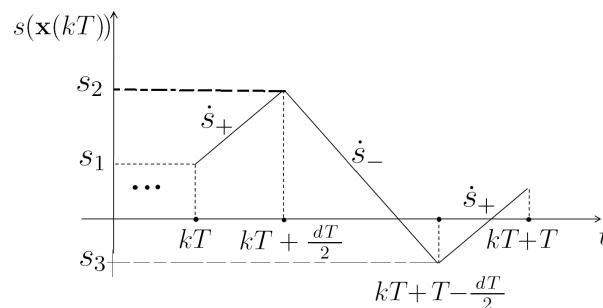


Figure 3. Commutation expressed in sections

The condition of the average zero is expressed in (8).

$$\int_{kT}^{(k+1)T} s(\mathbf{x}(kT)) dt = 0 \quad (8)$$

From (8), it is noted that the first and third slopes have the same values. All the information to build $s(\mathbf{x}(kT))$ is obtained from the state values x_1 and x_2 in the instant kT .

Solving the equation related with the condition of average zero (8), the expression for the duty cycle can be expressed as shown in (9).

$$d_k(kT) = \frac{2s_1(kT) + T\dot{s}_-(kT)}{T(\dot{s}_-(kT) - \dot{s}_+(kT))} \quad (9)$$

As in the experimental test, the variables are measured, the data are processed, and a CPWM is calculated with a frequency of 10 kHz with a one-delay period; thus, the expression of the duty cycle is defined

as in (10). This implies that the control law in the current period is calculated with the values of the states measured in the previous iteration.

$$d_k(kT) = \frac{2s_1((k-1)T) + T\dot{s}_-((k-1)T)}{T(\dot{s}_-((k-1)T) - \dot{s}_+((k-1)T))} \quad (10)$$

4. FPIC TECHNIQUE

FPIC was first presented in [20]. Later, a numerical test was performed in [19, 21] and finally the first experimental results were presented in [12]. In this section, the basis of the FPIC is presented.

4.1. FPIC theorem

Consider a system with a set of equations as shown in 11, where: $x(t) \in \mathbb{R}^n$ and $f : \mathbb{R}^n \rightarrow \mathbb{R}^n$.

$$x(k+1) = f(x(k)) \quad (11)$$

Suppose that a fixed point x^* exists that is unstable and within the orbit of control; that means $x^* = f(x^*)$. Suppose also that $J = \frac{\partial f}{\partial x}$ is the Jacobian of the system and that under this condition the system eigenvalues λ_i can be calculated. Then, when system is unstable, there is at least one i where $|\lambda_i(J)| > 1$. Thus, (12) guarantees stabilization in a fixed point when the parameter N has a real positive value.

$$x(k+1) = \frac{f(x(k)) + Nx^*}{N+1} \quad (12)$$

4.2. Demonstration

Initially, it should be noted that in (11), the fixed point has not been altered. In this case, the Jacobian of the new system can be expressed as shown in (13).

$$J_c = \frac{1}{N+1} J \quad (13)$$

where J_c is the Jacobian of the controlled system and J is the Jacobian of the unstable system. Therefore, a correct assignation of the parameter N guarantees stabilization at an equilibrium point, because the eigenvalues of the controlled system will be the eigenvalues of the original system divided by the factor $N+1$. One way to calculate directly N is through the Jury stability criterion. Then, by considering the strategy of ZAD and FPIC, a new duty cycle can be calculated with (14).

$$d_{ZADFPIC}(kT) = \frac{d_k(kT) + Nd^*}{N+1} \quad (14)$$

where $d_k(kT)$ is calculated from (10) and d^* . The value is calculated at the start of each period as in (15).

$$d^* = d_k(kT) |_{steady\ state} \quad (15)$$

Thus, (14) includes the ZAD and FPIC techniques. Considering that the duty cycle (d) must be greater than zero and less than 1, a new equation that corresponds to the saturation of the duty cycle is shown in (16).

$$d = \begin{cases} d_{ZADFPIC}(kT) & \text{if } 0 < d_{ZADFPIC}(kT) < 1 \\ 1 & \text{if } 1 \leq d_{ZADFPIC}(kT) \\ 0 & \text{if } d_{ZADFPIC}(kT) \leq 0 \end{cases} \quad (16)$$

5. FIRST MODEL OF THE BUCK CONVERTER

The classical model of the buck converter is represented in Figure 4. It consists of a switch, a diode, a filter LC , and a resistance representing the load (R). The DC source used in this case is regulated (E). However, authors of [19] demonstrated that when using the FPIC in the buck converter, the effects of the

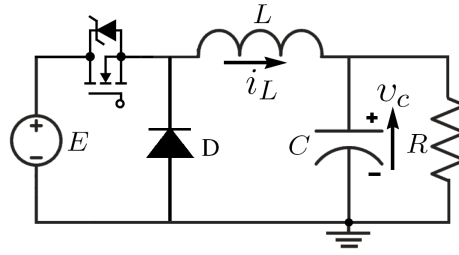


Figure 4. First model of the buck converter

regulated source can be neglected. In the experiments performed in this research, we used a switched source with nominal current of 6 A and variable voltage (0-80 VDC).

To obtain the mathematical model represented by equations in the state space, the resulting topologies generated due to the switching must be considered. On the one hand, when $u = u_1 = 1$, $u = u_2 = 0$, and the inductor current is positive, then a CCM is presented. On the other hand, when $u = u_2 = 0$ and the inductor current is zero, then a discontinuous conduction mode (DCM) is presented.

The converter has two energy storage elements (capacitor and inductor) and the state space model has two state variables: the capacitor voltage (v_c) and the inductor current (i_L). For the case of CCM, the representation of the state space is obtained with (17).

$$\begin{bmatrix} \dot{v}_c \\ \dot{i}_L \end{bmatrix} = \begin{bmatrix} -\frac{1}{RC} & \frac{1}{C} \\ -\frac{1}{L} & 0 \end{bmatrix} \begin{bmatrix} v_c \\ i_L \end{bmatrix} + \begin{bmatrix} 0 \\ \frac{E}{L} \end{bmatrix} u \quad (17)$$

The system described in (17) can be simplified as shown in (18).

$$\begin{bmatrix} \dot{x}_1 \\ \dot{x}_2 \end{bmatrix} = \begin{bmatrix} a & h \\ m & 0 \end{bmatrix} \begin{bmatrix} x_1 \\ x_2 \end{bmatrix} + \begin{bmatrix} 0 \\ \frac{E}{L} \end{bmatrix} u \quad (18)$$

where $x_1 = v_c$, $x_2 = i_L$, $a = -1/RC$, $h = 1/C$ and $m = -1/L$. The DCM is presented when the switch is open and the inductor current is equal to zero. In this case, the diode stops conducting and the capacitor is discharged through resistor R . The equation that models the dynamics of this topology is given by (19). It is important to note that although $i_L = 0$, the complete control of the output is not achieved; therefore, the control action is lost until a cycle begins.

$$\frac{dx_1}{dt} = ax_1, \quad \text{with } x_2 = 0 \quad (19)$$

Considering that the system operates in CCM, it can be represented as $\dot{x} = Ax + Bu$; where $\dot{x} = [\dot{x}_1, \dot{x}_2]'$ and $x = [x_1, x_2]'$. Because the control signal u has two values u_1 and u_2 , two different topologies for each sampling period are presented. This system is controlled by the CPWM and the model can be expressed as in (20).

$$\dot{x} = \begin{cases} Ax + Bu_1 & \text{if } kT \leq t \leq kT + dT/2 \\ Ax + Bu_2 & \text{if } kT + dT/2 < t < kT + T - dT/2 \\ Ax + Bu_1 & \text{if } kT + T - dT/2 < t < kT + T \end{cases} \quad (20)$$

5.1. Analytical solution for the first model

Some sections of the system shown in (20) are linear and time invariant [17, 19]. Thus, each section has a linear system in the form $\dot{x} = Ax + Bu$, which is solved analytically by using (21).

$$x(t) = e^{At}x(0) + \int_0^t e^{A(t-\tau)}Bu(\tau)d\tau \quad (21)$$

After solving each section of (21), the solution in the continuous time is defined as in (22).

$$x(t) = \begin{cases} e^{At}M_1 - A^{-1}B & \text{if } kT \leq t \leq (k + d/2)T \\ e^{At}M_2 & \text{if } (k + d/2)T < t < (k + 1 - d/2)T \\ e^{At}M_3 - A^{-1}B & \text{if } (k + 1 - d/2)T \leq t \leq (k + 1)T \end{cases} \quad (22)$$

where:

$$\begin{aligned} M_1 &= x(0) + A^{-1}B \\ M_2 &= M_1 - e^{-AT\frac{d}{2}}A^{-1}B \\ M_3 &= M_2 + e^{-AT(1-\frac{d}{2})}A^{-1}B \end{aligned} \quad (23)$$

The solution for the system in DCM is given by (24) and is possible when the inductor current is equal to zero.

$$\begin{bmatrix} x_1(t) \\ x_2(t) \end{bmatrix} = \begin{bmatrix} x(0)e^{-\frac{1}{RC}t} \\ 0 \end{bmatrix} \quad (24)$$

Starting from the solution in continuous time given in (22) and performing discretization in the output signals for each sampling period T , the following expression in discrete time [19] is given by (25), which is the solution in CCM for the studied converter.

$$x((k + 1)T) = e^{AT}x(kT) + [e^{AT} - e^{AT(1-\frac{d}{2})} + e^{AT\frac{d}{2}} - I]A^{-1}B \quad (25)$$

The solution for the system in DCM during the discrete time is given by (26).

$$\begin{bmatrix} x_1((k + 1)T) \\ x_2((k + 1)T) \end{bmatrix} = \begin{bmatrix} x_1(kT)e^{-\frac{1}{RC}T} \\ 0 \end{bmatrix} \quad (26)$$

5.2. ZAD control

Following the procedure described in Section 3. and considering a time delay, the duty cycle with the ZAD is calculated as shown in (27).

$$d_k(kT) = \frac{2s_1((k - 1)T) + T\dot{s}_-((k - 1)T)}{T(\dot{s}_-((k - 1)T) - \dot{s}_+((k - 1)T))} \quad (27)$$

where:

$$\begin{aligned} s_1((k - 1)T) &= (1 + ak_s)x_1((k - 1)T) + k_shx_2((k - 1)T) - x_{1ref} \\ \dot{s}_+((k - 1)T) &= (a + a^2k_s + k_shm)x_1((k - 1)T) + (h + ak_sh)x_2((k - 1)T) + k_sh\frac{E}{L} \\ \dot{s}_-((k - 1)T) &= (a + a^2k_s + k_shm)x_1((k - 1)T) + (h + ak_sh)x_2((k - 1)T) \end{aligned} \quad (28)$$

5.3. FPIC control

In the steady state $x_1 = x_{1ref}$ and $\dot{x}_1 = \dot{x}_{1ref} = 0$. With the last definition, the following consideration is obtained: $s(x(t)) = 0$. From the first equation of the system, $\dot{x}_1 = ax_1 + hx_2$, is obtained that $x_2 = (\dot{x}_{1ref} - ax_{1ref})/h$. Therefore, when regulation is considered, the expressions $x_1^* = x_{1ref}$ and $x_2^* = (\dot{x}_{1ref} - ax_{1ref})/h$ for the steady state are calculated. Then, x_1^* and x_2^* are the new state variables, depending only on the reference signal x_{1ref} and its derivate \dot{x}_{1ref} .

Replacing x_1^* and x_2^* in (27) and the parameters of the model (17), the duty cycle is calculated as in (29).

$$d^* = \left[\frac{x_{1ref}}{E_{measured}} \right] \quad (29)$$

5.4. ZAD-FPIC control

To control the converter with the ZAD and FPIC techniques, equation (30) is used, where N is the control parameter of the FPIC technique.

$$d_{ZADFPIC}(kT) = \frac{d_k(kT) + N \cdot d^*}{N + 1} \quad (30)$$

Thus, (30) includes both the ZAD (27, 28) and FPIC techniques (29). Considering that the duty cycle must be greater than zero and less than 1, then d can be expressed as in (31).

$$d = \begin{cases} d_{ZADFPIC}(kT) & \text{si } 0 < d_{ZADFPIC}(kT) < 1 \\ 1 & \text{si } 1 \leq d_{ZADFPIC}(kT) \\ 0 & \text{si } d_{ZADFPIC}(kT) \leq 0 \end{cases} \quad (31)$$

5.5. Stability analysis

This section determines the stability of the periodic orbit $1T$ for the first model of the buck converter controlled by the ZAD and FPIC with LEs. The LEs are a very powerful tool that helps to determine the convergence of two orbits of a recurrent equation whose initial conditions differ infinitesimally from one another.

Because knowledge of the orbits is required, the analytical calculation becomes very complex. Thus, a numerical procedure is preferred to find them. On one hand, when trajectories are very close to convergence, the associated LEs will be negative. On the other hand, when trajectories diverge, then at least one of the LEs is positive [22]. LEs are directly calculated from the Poincaré application given in (25) and rewritten in (32).

$$x((k+1)T) = e^{AT} x(kT) + [e^{AT} - e^{AT(1-\frac{d}{2})} + e^{AT\frac{d}{2}} - I]A^{-1}B \quad (32)$$

Equation (32) can be simplified as $\mathbf{x}(k+1) = \mathbf{F}(\mathbf{x}(k))$.

In the functioning scheme with a time delay ($n = 1$), the system presents four state variables (two current time variables and two delay time variables). This is because the duty cycle $d_k(kT)$ calculated with the ZAD is obtained with the samples measured in $(k-1)T$, as shown in (27); thus, when applying the ZAD and FPIC techniques, the following expressions are used for (28)-(31).

Therefore, the solution of the system $\mathbf{x}(k+1) = \mathbf{F}(\mathbf{x}(k))$ can be expressed as shown in (33).

$$\begin{aligned} x_1(k+1) &= f_1(x_1(k), x_2(k), x_3(k), x_4(k)) \\ x_2(k+1) &= f_2(x_1(k), x_2(k), x_3(k), x_4(k)) \\ x_3(k+1) &= x_1(k) \\ x_4(k+1) &= x_2(k) \end{aligned} \quad (33)$$

where f_1 is the discrete solution in the time for v_c , f_2 is the discrete solution in the time for i_L , $x_3(k+1)$, and $x_4(k+1)$ are the variables v_c and i_L in the previous instant (k).

The Jacobian of the system is given by (34).

$$DF(\mathbf{x}(k)) = \begin{bmatrix} \frac{\partial f_1}{\partial x_1(k)} & \frac{\partial f_1}{\partial x_2(k)} & \frac{\partial f_1}{\partial x_3(k)} & \frac{\partial f_1}{\partial x_4(k)} \\ \frac{\partial f_2}{\partial x_1(k)} & \frac{\partial f_2}{\partial x_2(k)} & \frac{\partial f_2}{\partial x_3(k)} & \frac{\partial f_2}{\partial x_4(k)} \\ 1 & 0 & 0 & 0 \\ 0 & 1 & 0 & 0 \end{bmatrix} \quad (34)$$

The term $q_i(DF(x))$ is the i -eigenvalue of $DF(\mathbf{x}(k))$. The LE λ_i of the respective eigenvalue is given by (35).

$$\lambda_i = \lim_{n \rightarrow \infty} \left\{ \frac{1}{n} \sum_{k=0}^n \log |q_i(DF(x))| \right\} \quad (35)$$

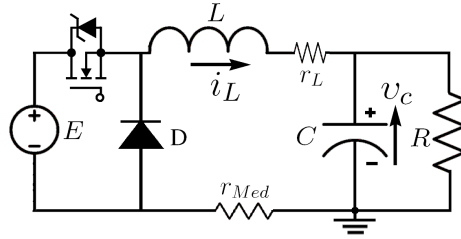


Figure 5. Second model of the buck converter

6. SECOND MODEL OF THE BUCK CONVERTER

In this second model, the losses are considered by adding an inductor r_L and a resistance used to measure the current r_{Med} as shown in Figure 5. Therefore, r_{Med} was considered with an approximate value of 1.007Ω .

The mathematical model of the CCM is described in (36).

$$\begin{bmatrix} \dot{v}_c \\ \dot{i}_L \end{bmatrix} = \begin{bmatrix} \frac{-1}{RC} & \frac{1}{C} \\ \frac{-1}{L} & \frac{-(r_{Med} + r_L)}{L} \end{bmatrix} \begin{bmatrix} v_c \\ i_L \end{bmatrix} + \begin{bmatrix} 0 \\ \frac{E}{L} \end{bmatrix} u \quad (36)$$

The system (36) can be simplified and expressed as shown in (37), where $x_1 = v_c$, $x_2 = i_L$.

$$\begin{bmatrix} \dot{x}_1 \\ \dot{x}_2 \end{bmatrix} = \begin{bmatrix} a & h \\ m & p \end{bmatrix} \begin{bmatrix} x_1 \\ x_2 \end{bmatrix} + \begin{bmatrix} 0 \\ \frac{E}{L} \end{bmatrix} u \quad (37)$$

The system in CCM can be represented similar to the model in (5.), according to the simplified form $\dot{x} = Ax + Bu$. As with the simplified model, this system can be represented with the simple equation shown in (38).

$$\dot{x} = \begin{cases} Ax + Bu_1 & \text{if } kT \leq t \leq kT + dT/2 \\ Ax + Bu_2 & \text{if } kT + dT/2 < t < kT + T - dT/2 \\ Ax + Bu_1 & \text{if } kT + T - dT/2 < t < kT + T \end{cases} \quad (38)$$

In the DCM, the system is modeled in the same way as for the first model of the buck converter as shown in (19). The analytical solutions for the continuous case and the discrete case are the same as the solution for the first model and are given by (22), (24), (25) and (26). In this case, the matrix of the state transition e^{AT} is changed, which is affected by the internal resistances r_L and r_{Med} .

6.1. ZAD-FPIC control for the second model of buck converter

The procedure to apply the ZAD technique is the same as described in Section 3. With this procedure, the mathematical expression shown in (39) is obtained.

$$d_k(kT) = \frac{2s_1((k-1)T) + T\dot{s}_-((k-1)T)}{T(\dot{s}_-((k-1)T) - \dot{s}_+((k-1)T))} \quad (39)$$

where:

$$\begin{aligned} s_1((k-1)T) &= (1 + ak_s)x_1((k-1)T) + k_s h x_2((k-1)T) - x_{1ref} \\ \dot{s}_+((k-1)T) &= (a + a^2 k_s + k_s h m)x_1((k-1)T) + \\ &\quad (h + ak_s h + k_s h p)x_2((k-1)T) + k_s h \frac{E}{L} \\ \dot{s}_-((k-1)T) &= (a + a^2 k_s + k_s h m)x_1((k-1)T) + \\ &\quad (h + ak_s h + k_s h p)x_2((k-1)T) \end{aligned} \quad (40)$$

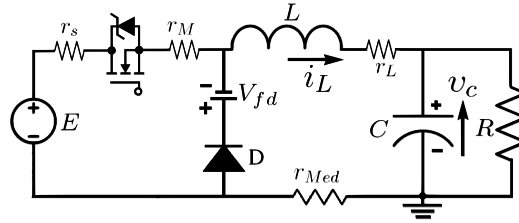


Figure 6. Third model of the buck converter

For the FPIC technique, the procedure described in Section 5.3. is used. Then, the equation shown in (41) is obtained.

$$d^* = x_{1ref} \cdot \left[\frac{1 + \frac{r_L + r_{Med}}{R}}{E_{measured}} \right] \quad (41)$$

6.2. Stability analysis

As in the first model of the buck converter, stability analysis for the second model of the buck converter is performed by using LEs. The procedure is the same as described in Section 5.5.

7. THIRD MODEL OF THE BUCK CONVERTER

For this model, other types of losses are included for the buck converter model by considering the resistance of the source (r_s) and the resistance of the MOSFET (r_M) as shown in Figure 6. The internal resistance of the source is increased due to the resistances of the contacts, cables, series switch, and shut-down converter.

The MOSFET resistance r_M and the forward voltage in the fast diode V_{fd} were taken from datasheets. Additionally, the internal resistance was measured in a laboratory test.

For the control input $u = u_1 = 1$, the equation in the state space is given as in (42). In a simplified way, this equation can be expressed as in (43). When the switch is open ($u = u_2 = 0$), the system is modeled as in (44) and simplified as in (45).

$$\begin{bmatrix} \dot{v}_c \\ \dot{i}_L \end{bmatrix} = \begin{bmatrix} \frac{-1}{RC} & \frac{1}{C} \\ \frac{-1}{L} & \frac{-(r_s + r_M + r_{Med} + r_L)}{L} \end{bmatrix} \begin{bmatrix} v_c \\ i_L \end{bmatrix} + \begin{bmatrix} 0 \\ \frac{E}{L} \end{bmatrix} \quad (42)$$

$$\begin{bmatrix} \dot{x}_1 \\ \dot{x}_2 \end{bmatrix} = \begin{bmatrix} a & h \\ m & p_2 \end{bmatrix} \begin{bmatrix} v_c \\ i_L \end{bmatrix} + \begin{bmatrix} 0 \\ \frac{E}{L} \end{bmatrix} \quad (43)$$

$$\begin{bmatrix} \dot{v}_c \\ \dot{i}_L \end{bmatrix} = \begin{bmatrix} \frac{-1}{RC} & \frac{1}{C} \\ \frac{-1}{L} & \frac{-(r_{Med} + r_L)}{L} \end{bmatrix} \begin{bmatrix} v_c \\ i_L \end{bmatrix} + \begin{bmatrix} 0 \\ \frac{-V_{fd}}{L} \end{bmatrix} \quad (44)$$

$$\begin{bmatrix} \dot{x}_1 \\ \dot{x}_2 \end{bmatrix} = \begin{bmatrix} a & h \\ m & p_3 \end{bmatrix} \begin{bmatrix} v_c \\ i_L \end{bmatrix} + \begin{bmatrix} 0 \\ \frac{-V_{fd}}{L} \end{bmatrix} \quad (45)$$

where $x_1 = v_c$, $x_2 = i_L$.

For the CCM, these equations have been simplified as shown in (46), where the term $\dot{x} = [\dot{x}_1, \dot{x}_2]'$ = $[\frac{dx_1}{dt}, \frac{dx_2}{dt}]'$, B_1 , and B_2 consider the information of the control input such as the voltage source (E) and direct polarization voltage of the diode ($-V_{fd}$). Likewise the previous cases, the system controlled by the CPWM operates as expressed in (46).

$$\dot{x} = \begin{cases} A_1x + B_1 & \text{if } kT \leq t \leq kT + dT/2 \\ A_2x + B_2 & \text{if } kT + dT/2 < t < kT + T - dT/2 \\ A_1x + B_1 & \text{if } kT + T - dT/2 < t < kT + T \end{cases} \quad (46)$$

7.1. Analytical solution for the third model of the buck converter

The system operating in CCM has the solution in continuous time given by (47).

$$x(t) = \begin{cases} e^{A_1 t} M_1 - V_1 & \text{si } kT \leq t \leq (k + d/2)T \\ e^{A_2 t} M_2 - V_2 & \text{si } (k + d/2)T < t < (k + 1 - d/2)T \\ e^{A_1 t} M_3 - V_1 & \text{si } (k + 1 - d/2)T \leq t \leq (k + 1)T \end{cases} \quad (47)$$

where:

$$\begin{aligned} M_1 &= x(0) + V_1 \\ M_2 &= Q_{12} M_1 - \Delta V e^{-A_2 T \frac{d}{2}} \\ M_3 &= Q_{21} M_2 + \Delta V e^{-A_1 T (1 - \frac{d}{2})} \\ Q_{12} &= e^{(A_1 - A_2) T (\frac{d}{2})} \\ Q_{21} &= e^{(A_2 - A_1) T (1 - \frac{d}{2})} \\ V_1 &= A_1^{-1} B_1 \\ V_2 &= A_2^{-1} B_2 \\ \Delta V &= V_1 - V_2 \end{aligned} \quad (48)$$

The solution of the system in DCM is given in (49) and it occurs when the inductor current is equal to zero.

$$\begin{bmatrix} x_1(t) \\ x_2(t) \end{bmatrix} = \begin{bmatrix} x(0) e^{-\frac{1}{RC} t} \\ 0 \end{bmatrix} \quad (49)$$

Starting from the solution in the continuous time given in (47) and performing discretization in the output signals for each sampling period T , the following expression is obtained in (50), which is a stroboscope map of the solution in CCM for the third model.

$$x((k + 1)T) = e^{A_1 T} Q x(kT) + e^{A_1 T} Q V_1 - Q_{12} e^{A_2 T (1 - \frac{d}{2})} \Delta V + e^{A_1 T \frac{d}{2}} \Delta V - V_1 \quad (50)$$

The matrix Q is given in (51) and the other expressions are given in (48).

$$Q = e^{(A_2 - A_1) T} e^{(A_1 - A_2) T d} \quad (51)$$

The solution of the system for the DCM in the discrete time is given by (52).

$$\begin{bmatrix} x_1((k + 1)T) \\ x_2((k + 1)T) \end{bmatrix} = \begin{bmatrix} x_1(kT) e^{-\frac{1}{RC} T} \\ 0 \end{bmatrix} \quad (52)$$

7.2. ZAD-FPIC control for the third model of the buck converter

The necessary steps to apply the ZAD control technique are the same described in Section 3. It is important to consider that when the topology changes through the action of the switch, the state matrices of the system and the input arrays also change.

The duty cycle with the ZAD technique is calculated as in (53).

$$d_k(kT) = \frac{2s_1((k - 1)T) + T\dot{s}_-((k - 1)T)}{T(\dot{s}_-((k - 1)T) - \dot{s}_+((k - 1)T))} \quad (53)$$

where,

$$\begin{aligned} s_1((k - 1)T) &= (1 + ak_s)x_1((k - 1)T) + k_s h x_2((k - 1)T) - x_{1ref} \\ \dot{s}_+((k - 1)T) &= (a + a^2 k_s + k_s h m)x_1((k - 1)T) + \\ &\quad (h + ak_s h + k_s h p_2)x_2((k - 1)T) + k_s h \frac{E}{L} \\ \dot{s}_-((k - 1)T) &= (a + a^2 k_s + k_s h m)x_1((k - 1)T) + \\ &\quad (h + ak_s h + k_s h p_3)x_2((k - 1)T) - k_s h \frac{V_{fd}}{L} \end{aligned} \quad (54)$$

When the FPIC control technique is used, then the procedure described in Section 4. must be considered and the equation shown in (55) is obtained.

$$d^* = \left[\frac{x_{1ref} \cdot \left(1 + \frac{r_{Med} + r_L}{R}\right) + V_{fd}}{-x_{1ref} \cdot \left(\frac{r_s + r_M}{R}\right) + E_{measured} + V_{fd}} \right] \quad (55)$$

7.3. Stability analysis

As in the first and second model of the buck converter, the stability analysis for the third model of the buck converter is performed by using LEs. The procedure is the same as described in Section 5.5. For this case, the LEs are directly calculated by using the application of Poincaré.

8. RESULTS AND ANALYSIS

In this section, comparisons between the theoretical, simulation, and experimental tests for the ZAD and FPIC techniques are performed. The theoretical test considers the evaluation of stability with LEs, the simulation test is performed by using the Poincaré map, and the experimental test is performed by using an electronic circuit.

8.1. Parameters for the test

The software used for programming the controllers is developed in the control board and DS1104 of dSPACE GmbH. In this board, the ZAD and FPIC were implemented and programmed with the MATLAB-Simulink and ControlDesk software. The controller was implemented in Simulink and uploaded to the DS1104 in order to work as a real-time application. The parameters for all the models are shown in Table 1. All the parameters included were used to build the circuit and compare the results with the models of the theoretical and simulation tests. The effects of the quantization come from the control board and the DS1104, where the controller was implemented with 12 bits for the analogue signals measured in the test v_c and i_L . The duty cycle d was considered as 10 bits.

Table 1. Parameters for the three models of the buck converter controlled by the ZAD and FPIC

Parameter	Description	Value
r_s	Internal resistance of the source	0.3887 Ω
r_M	MOSFET resistance	0.3 Ω
V_{fd}	Forward voltage	1.1 V
r_{Med}	Resistance of the measurement i_L	1.007 Ω
r_L	Internal resistance of the inductor	0.338 Ω
v_{ref}	Reference voltage	32 V
E	Voltage of the source	40.086 V (switched source)
R	Resistance of the load	39.3 Ω
C	Capacitance	46.27 μF
L	Inductance	2.473 mH
N	Parameter of the FPIC control	1
K_s	Parameter of bifurcation	Variable between 0 and 5
F_c	Switched frequency	10 kHz
F_s	Sampling frequency	10 kHz
$1T_p$	Delay time	100 μs

8.2. Results for the first model

Figure 7 shows the stability analysis and the comparison between the theoretical, simulation, and experimental tests for the first model of the buck converter controlled by the ZAD and FPIC. Figure 7a shows the

evolution of the LEs with the mathematical solution. Figure 7b shows the bifurcation diagram obtained with the numerical analysis of the controlled variables v_c versus K_s using a Poincaré map. Figure 7c shows the bifurcation diagram for the experimental test with the implemented electronic circuit. The stability behaviors shown for the two first figures were created by changing the control parameter K_s from 0 to 100 and maintaining the control parameter N equal to 1. The stability behavior shown in the third figure was created by changing the control parameter K_s from 0 to 5 and maintaining the control parameter N equal to 1. The term v_c is the capacitor voltage or the output voltage, the visualization range of which was maintained between 28 V and 36 V.

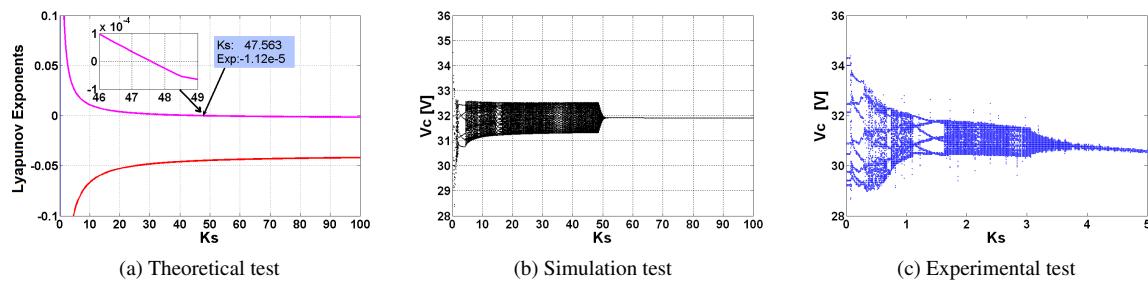


Figure 7. Stability of the first model controlled by the ZAD and FPIC

Using this mathematical method, the bifurcation point, the trace of the stability behavior, and the stability zones were detected and plotted (Figure 7a). The point $K_s = 47.563$ represents a stability limit, where the greater values of K_s represent the stable zone and the lower values of K_s represent the unstable zone.

The simulations confirm that there is a stability zone (right side of Figure 7b) and an instability zone with a limit point close to that determined with the mathematical model. In addition, an unstable zone and chaos are presented when the parameter K_s is decreased. The point determined with the theoretical analysis is validated as a point representing the stability limit of the system when $K_s \simeq 50$.

Similar to the previous results presented in this paper, the experimental test shows a stable zone (right side of Figure 7c) where the signals remain with low variations, and an unstable zone (left side of the Figure 7c) where the signals change abruptly. Comparison with the two previous figures show that the system can represent similar stability behavior. Besides, the controlled variable v_c is very close to the reference signal v_{ref} . From this figure, the diagram obtained with the simulation is shifted to the right with respect to the diagram of the experimental test. In addition, the chaos and periodicity zones are expanded on the axis K_s as shown in Figure 7b. Figure 7c shows for the experimental test that a stability limit is obtained when the controlled parameter is $K_s \simeq 3.75$. Therefore, the three figures show some coincidence and correlation when comparing the responses of the system as they represent similar events. However, the experimental test shows deviations with respect to theoretical and simulated tests when the parameter K_s changes. These deviations could be corrected by adding new elements that represent the losses of other elements in the system that are not considered in the simulation model.

8.3. Results for the second model

Figure 8 shows the stability analysis and the comparison between the theoretical, simulation, and experimental tests for the second model of the buck converter controlled by the ZAD and FPIC. As previously described, an internal resistance r_L and a resistance of measurement r_{Med} were added to the model. Figure 8a shows the evolution of the LEs with the mathematical solution. Figure 8b shows the bifurcation diagram obtained with the numerical analysis of the controlled variables v_c versus K_s by using a Poincaré map. Figure 8c shows the bifurcation diagram for the experimental test with the implemented electronic circuit. The stability behaviors shown in the three figures were created by changing the control parameter K_s from 0 to 5 and maintaining the control parameter N equal to 1. The term v_c is the capacitor voltage or the output voltage, the visualization range of which range was maintained between 28 V and 36 V.

The stability limit calculated with the LEs was reduced with respect to the results of the first model because with the elements added, some fixed stable points for values of $K_s \simeq 4.58$ are presented. The two

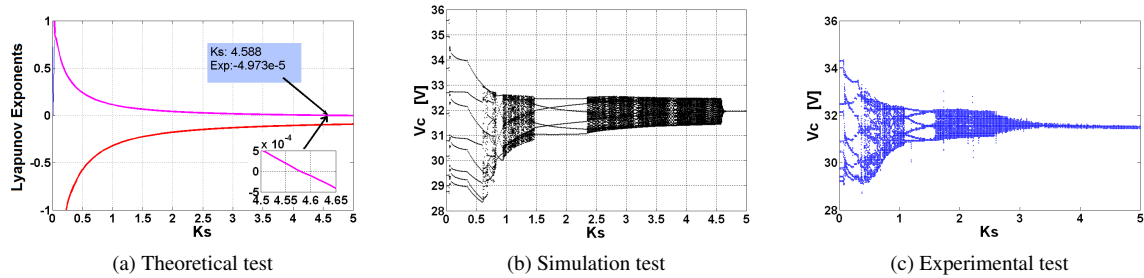


Figure 8. Stability of the second model controlled by the ZAD and FPIC

exponents become negative for values of $K_s > 4.588$. Therefore, the analysis determined that for this second model, the stability of the system is found for values of $K_s < 4.588$, which must be validated with other analyses. The bifurcation diagram is shifted to the left of the axis of the parameter K_s . The stability limit is represented close to the value obtained with the LEs. However, the signals in the instability zone are larger than the obtained with the mathematical calculation.

Therefore, by using the second model presented in this research, the three figures present more coincidence and correlation as they represent better the events when the parameter K_s is changed. Compared with the results of the first model, the bifurcation diagrams of the simulation and experimental test are more similar and represent more details of the events. However, the equilibrium point is shifted to the right with respect to the diagram of the experimental tests, although it is improved with respect to the first model. Therefore, by adding the internal resistance of the inductor r_L and a resistance for measuring the current r_{Med} , better similitude is presented between the simulation and experimental tests.

8.4. Results for the third model

Figure 9 shows the stability analysis and the comparison of the theoretical, simulation, and experimental test for the third model of the buck converter controlled by the ZAD and FPIC. As previously described, the additional parameters added to the model were r_s , r_M , and V_{fd} . First, Figure 9a shows the evolution of the LEs with the mathematical solution. Second, Figure 9b shows the bifurcation diagram obtained with the numerical analysis of the controlled variables v_c versus K_s , by using a Poincaré map. Finally, Figure 9c shows the bifurcation diagram for the experimental test with the implemented electronic circuit. The stability behaviors presented in the three figures were created by changing the control parameter K_s from 0 to 5 and maintaining the control parameter N equal to 1. The term v_c is the capacitor voltage or the output voltage, the visualization range of which was maintained between 28 V and 36 V.

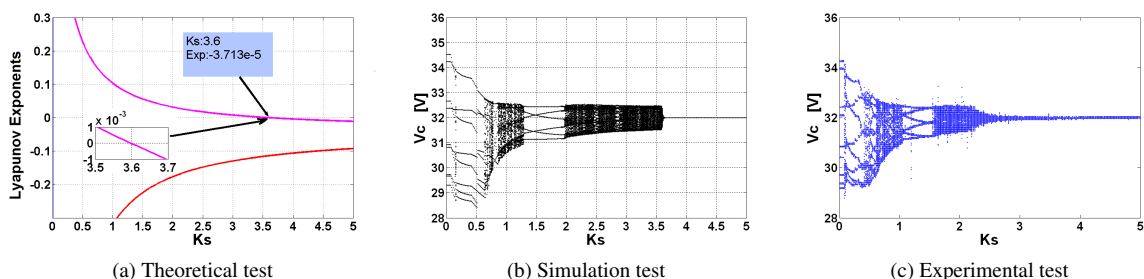


Figure 9. Stability of the third model controlled by the ZAD and FPIC

Because most of the losses are included with the inclusion of the parameters r_s , r_M , r_{Med} , and r_L , a regulated voltage is obtained with an error in the steady state lower than 0.2%. The bifurcation diagram obtained in the simulation test shows that the stability limit is obtained with a reduced K_s lower than that obtained in the second model, which is $K_s \approx 3.6$. Furthermore, it can be concluded that the results obtained

in the simulation test are more similar to those obtained in the experimental test, but some low differences are still found that will be investigated in future research.

The experimental test shows a small cloud of electromagnetic noise produced by the switch commutation; however, this noise can be neglected. In the results obtained by the simulation test, the stability limit is shifted to the right more than in the experimental test. This displacement can be attributed to some parameters not included in the model of the controller such as internal resistance, parasitic capacitances and parasitic inductances presented in the circuit, and the gains of the circuit used for setting the signal.

The results show that the LEs are negative for $K_s \geq 3.6$ in the theoretical test, which indicates the stability of the system and is similar to the results obtained in the simulation and experimental tests. The stability limit in the experimental test is obtained when $K_s \geq 2.7$, whereas for the simulation test it is $K_s \geq 3.6$. The number of bands and their behaviors illustrated in the figures are similar for both the simulation and experimental tests.

In the experimental test, when $K_s < 2.7$, the system slowly loses regulation capacity, starting with chaotic behavior. Next, some periodic bands appear and a new chaos proceeds and, finally, a chaotic band behavior occurs. For both the simulation and experimental tests, the error in regulation increases when the value of K_s is decreased.

Because most of resistive losses have been included, the diagrams obtained in simulation are very similar to the experimental test. In this case, it is clear that the controlled variable v_c reaches the reference when $K_s > 4$. Therefore, we can conclude that the third model is the best to represent similar events in the theoretical, simulation, and experimental tests.

8.5. Two-parameter bifurcation diagrams

Figures 10 and 11 show the two-parameter bifurcation diagrams for the three models of the buck converter controlled by ZAD and FPIC, and the third model with the quantization effects. The colors in this figure indicate the presence of multiple orbits due to the quantization noise.

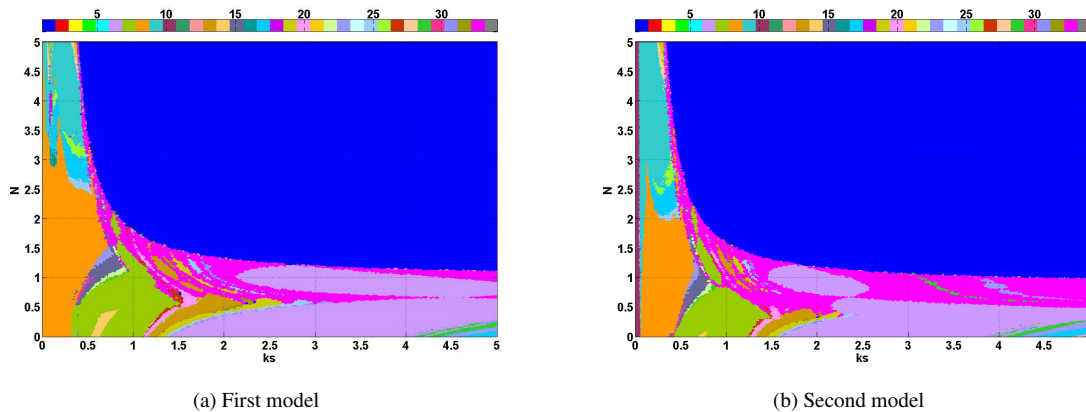


Figure 10. Two-parameter bifurcation diagrams for the (a) first model and (b) second model

Because the bifurcation diagrams have been created with $N=1$ and K_s changing between 0 and 5, the system operates in the stability limits between the fixed points and chaos, as observed in Figures 10a, 10b, and 11a. Although the results show good similitude between the simulation and experimental tests, there are some small differences in magnitude, time, and signal deviation that need to be investigated in future research by considering other parameters.

In general, the first three bifurcation diagrams of two parameters tend to be similar and the fourth tends to be similar to the two first ones but with some differences due to the quantization noise. The two-parameter bifurcation diagram including the quantization effects, as shown in Figure 11b, considered $N = 1$ and K_s between 0 and 5, which satisfies the regulation conditions (steady-state error $< 3\%$); thus, in this area, the system can operate under stability.

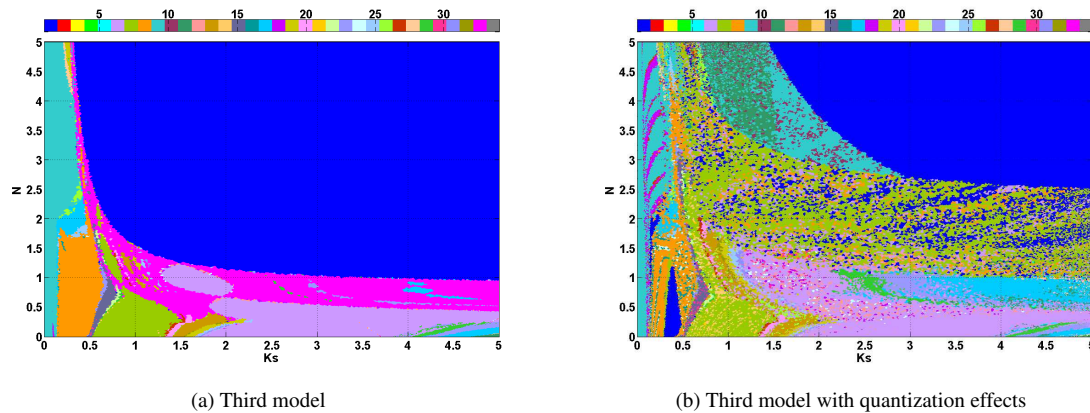


Figure 11. Two-parameter bifurcation diagrams for the (a) third model and (b) third model with quantization effects

9. CONCLUSIONS

This paper presented a detailed report of a theoretical analysis, control design and simulated and real responses of a power converter. If each process had been done separately, then the best model could not be found or the research would have been delayed. The integration of rapid control prototyping (RCP) processes with effective math tools, such as Lyapunov exponents and bifurcation diagrams, allowed the selection and validation of the most appropriate model.

The paper has presented a stability analysis for the classical and two modified buck converter models controlled by ZAD and FPIC. Mathematical representations of the buck converters with the controllers were presented and the LEs were calculated. The theoretical results were compared with the simulation and experimental results by using one and two-parameter bifurcation diagrams. The quantization effects in the input variables and the signals of PWM were applied for the best model to identify the differences with the other three models. After these studies, we can conclude that the inclusion of the internal resistance r_L , r_s , and r_M , the system becomes more stable. Thus, the test that changes the parameter K_s shows that the equilibrium point is shifted to the left of the bifurcation diagram. The stability of the periodic orbit $1T$ for the three models of the buck converters controlled by ZAD and FPIC were determined by using LEs. When the number of bits of the measured signals and the duty cycle are decreased, the system starts losing stability, presents dynamic behaviors such as periodic bands and chaos, and becomes more chaotic. It is important to note that even with a low number of bits in the input variables and the duty cycle, the system controlled by ZAD and FPIC follows the reference signal with low error ($< 3\%$) in the steady state.

The most elaborate model is not always the most accurate. In our illustrative case, the model that includes the effects of quantization does not achieve a better correspondence between experimental and simulated performance. We recommend gradually varying the model until a tolerable level of difference is sensed between experimental and simulated tests. The stages of modeling, control design and experimental validation should be integrated because in many cases, non-modeled dynamics could influence the calibration of the control system and the closed-loop responses.

ACKNOWLEDGEMENT

The authors thank to the School of Physics, and the Department of Electrical Engineering and Automation for the valuable support to conduct this research. This work was supported by the Universidad Nacional de Colombia, Sede Medellín under the projects HERMES-34671 and HERMES-36911.

REFERENCES

- [1] Mehdi A, Rezgui S, Medouche H, Benalla H. "A Comparative Study between DPC and DPC-SVM Controllers Using dSPACE (DS1104)". *International Journal of Electrical and Computer Engineering*. 2014;

- 4(3): 322 – 328
- [2] Hoyos S, Candelo J, Silva J. “Performance evaluation of a DC-AC inverter controlled with ZAD-FPIC”. *INGE CUC*. 2018; 14(1): 9-18.
 - [3] Haitao H, Yousefzadeh V, Maksimovic D. “Nonuniform A/D quantization for improved dynamic responses of digitally controlled DC-DC converters”. *IEEE Transactions on Power Electronics*. 2008; 23: 1998-2005.
 - [4] Fung CW, Liu CP, Pong MH. “A diagrammatic approach to search for minimum sampling frequency and quantization resolution for digital control of power converters”. *IEEE Power Electronics Specialists Conference*. 2007: Orlando, Florida, USA.
 - [5] Taborda J, Angulo F, Olivar G. “Estimation of parameters in buck converter with digital-PWM control based on ZAD strategy”. *IEEE Second Latin American Symposium. Circuits and Systems (LASCAS)*. 2011; Bogotá, Colombia.
 - [6] Maksimovic D, Zane R, Erickson R. “Impact of digital control in power electronics”. *IEEE, the 16th International Symposium on Power Semiconductor Devices and ICs*. 2004, Kitakyushu, Japan.
 - [7] Peterchev A, Sanders S. “Quantization resolution and limit cycling in digitally controlled PWM converters”. *IEEE Transactions on Power Electronics*. 2003; 18: 301-308.
 - [8] Hao P, Maksimovic D, Prodic A, Alarcon E. “Modeling of quantization effects in digitally controlled DC-DC converters”. *IEEE, the 35th Ann. Power Electronics Specialists Conference*. 2004; Aachen, Germany.
 - [9] Angulo F, Hoyos F, Olivar G. “Experimental results on the quantization in the ADC device for a ZAD-strategy controlled DC-DC buck converter”. *7th European Nonlinear Dynamics Conference*. 2011; Rome, Italy.
 - [10] Tirandaz H, Ahmadnia M, Tavakoli H. “Adaptive Projective Lag Synchronization of T and Lu Chaotic Systems”. *International Journal of Electrical and Computer Engineering*. 2017; 7(6): 3446-3453.
 - [11] Corradini L, Mattavelli P. “Analysis of multiple sampling technique for digitally controlled DC-DC converters”. *37th IEEE Power Electronics Specialists Conference*, 2006; Jeju, Korea.
 - [12] Hoyos F, Burbano D, Angulo F, Olivar G, Toro N, Taborda J. “Effects of quantization, delay and internal resistances in digitally ZAD-controlled buck converter”. *International Journal of Bifurcation and Chaos*. 2012; 22(10): 1-9.
 - [13] Algreer M, Armstrong M, Giaouris D. “Adaptive PD+I control of a switch-mode DC-DC power converter using a recursive FIR predictor”. *IEEE Transactions on Industry Applications*. 2011; 47(5): 2135-2144. DOI: 10.1109/TIA.2011.2161856.
 - [14] Shirazi M, Zane R, Maksimovic D. “An autotuning digital controller for DC-DC power converters based on online frequency-response measurement”, *IEEE Transactions on Power Electronics*. 2009; 24(11): 2578-2588. DOI: 10.1109/TPEL.2009.2029691.
 - [15] Hoyos F, Toro N, García Y. “Adaptive control for buck power converter using fixed point inducting control and zero average dynamics strategies”. *International Journal of Bifurcation and Chaos*. 2015; 25(4): Issue 04, pages: 1-13.
 - [16] Bhat S, Nagaraja HN. “Effect of Parasitic Elements on the Performance of Buck-Boost Converter for PV Systems”. *International Journal of Electrical and Computer Engineering*. 2014; 4(6): 831-836.
 - [17] Fossas E, Griño R, Biel D. “Quasi-Sliding control based on pulse width modulation, zero averaged dynamics and the L2 norm”. *Proceedings of the 6th IEEE International Workshop on Variable Structure Systems: Advances in Variable Structure Systems*. 2000; 335-344.
 - [18] Parvathyshankar D, Simon A. “Chaotic dynamics of a zero average dynamics controlled DC-DC cuk converter”. *IET Power Electronics*. 2014; 7(2): 289-298.
 - [19] Angulo F, Olivar G, Taborda J, Hoyos F. “Nonsmooth dynamics and FPIC chaos control in a DC-DC ZAD-strategy power converter”. *ENOC*. Saint Petersburg - Russia. 2008; 1-6.
 - [20] Angulo F, Burgos JE, Olivar G. “Chaos stabilization with TDAS and FPIC in a buck converter controlled by lateral PWM and ZAD”. *Mediterranean Conference on Control and Automation*. 2007; 1-6. DOI: 10.1109/MED.2007.4433846.
 - [21] Taborda J, Santini S, Bernardo M.di, and Angulo F. “Active chaos control of a cam-follower impacting system using FPIC technique”. *IFAC Conference on Analysis and Control of Chaotic Systems*. 2009; 42(7): 327-332.
 - [22] Banerjee S, Verghese G.C. “Nonlinear phenomena in power electronics: Bifurcations, Chaos, Control, and Applications”. *Wiley-IEEE Press*, 2001.

BIOGRAPHIES OF AUTHORS

Fredy Edimer Hoyos Electrical Engineer, MEng Industrial Automation, Ph.D on Automation. Assistant professor, Science Faculty, School of Physics, Universidad Nacional de Colombia Sede Medellín, Colombia, E-mail: fehoyosve@unal.edu.co. His research interests include nonlinear control, nonlinear dynamics of nonsmooth systems, and power electronic applications. He is a member of the Scientific and Industrial Instrumentation Research Group, at the Universidad Nacional de Colombia. <https://orcid.org/0000-0001-8766-5192>



John Candelo received his Bs. degree in Electrical Engineering in 2002 and his PhD in Engineering with emphasis in Electrical Engineering in 2009 from Universidad del Valle, Cali - Colombia. His employment experiences include the Empresa de Energía del Pacífico EPSA, Universidad del Norte, and Universidad Nacional de Colombia - Sede Medellín. He is now an Assistant Professor of the Universidad Nacional de Colombia - Sede Medellín, Colombia. His research interests include: engineering education; planning, operation and control of power systems; artificial intelligence; and smart grids. <https://orcid.org/0000-0002-9784-9494>.



John Alexander Taborda Electronics Engineer, MEng Industrial Automation, Ph.D on Automation. Associated professor, Engineering Faculty, Universidad del Magdalena, Santa Marta, Colombia, E-mail: jtaborda@unimagdalena.edu.co. His research interests include applied mathematics, complex dynamical systems, chaos and control theories, and power electronic applications. He is a senior researcher in Colciencias and member of research group Magma Ingeniería at the Universidad del Magdalena. <http://orcid.org/0000-0002-6090-1711>